International Journal of Information, Control and Computer Sciences
ISSN: 2517-9942
Vol:7, No:4, 2013

Localization of Anatomical Landmarks in Head CT Images for Image to Patient Registration

M. Ovinis, D. Kerr, K. Bouazza-Marouf, M. Vloeberghs

***Abstract*—**The use of anatomical landmarks as a basis for image to patient registration is appealing because the registration may be performed retrospectively. We have previously proposed the use of two anatomical soft tissue landmarks of the head, the canthus (corner of the eye) and the tragus (a small, pointed, cartilaginous flap of the ear), as a registration basis for an automated CT image to patient registration system, and described their localization in patient space using close range photogrammetry. In this paper, the automatic localization of these landmarks in CT images, based on their curvature saliency and using a rule based system that incorporates prior knowledge of their characteristics, is described. Existing approaches to landmark localization in CT images are predominantly semi-automatic and primarily for localizing internal landmarks. To validate our approach, the positions of the landmarks localized automatically and manually in near isotropic CT images of 102 patients were compared. The average difference was 1.2mm (std = 0.9mm, max = 4.5mm) for the medial canthus and 0.8mm (std = 0.6mm, max = 2.6mm) for the tragus. The medial canthus and tragus can be automatically localized in CT images, with performance comparable to manual localization, based on the approach presented.

***Keywords*—**Anatomical Landmarks, CT, Localization.

I. Introduction

THE Mechatronics in Medicine group at Loughborough University, UK is developing a supervisory-controlled robotic system for emergency neurosurgery. Under our proposed protocol, an off-site neurosurgeon will provide a preoperative plan based on computed tomography (CT) images of the patient, to guide the surgical intervention by the robot. Spatial correspondence between the preoperative plan and the patient will be established through a technique known as image-to-patient registration. The use of fiducial markers, which is the method of choice for image-to-patient registration systems, requires a secondary scan, which may delay time to surgery and may not always be possible. On the other hand, registration may be performed retrospectively based on the initial diagnostic scans of a patient if anatomical landmarks are used. We have previously proposed the use of the canthus and tragus as a basis for an automated CT image to patient registration system and described their localization, using close range photogrammetry, in patient space [1]. These landmarks were chosen as they are the most geometrically salient among commonly used anatomical landmarks of the head and can therefore be more reliably detected in an automated system.

The medial canthus (Fig. 1 (a)) is the inner corner of the eye where the upper and lower eyelids meet. The tragus is a small, pointed, cartilaginous flap in front of the external opening of the ear. Because the tragus is a relatively large structure, its apex is chosen as the point that uniquely defines its position (Fig. 1 (b)). The use of these landmarks avoids resorting to surface analogues of bone landmarks such as the soft tissue nasion, which can usually only be found in patient space through palpation. Although these landmarks may be localized manually on surface models extracted from CT images, as these images are digital in nature, a computational approach for their localization was developed.

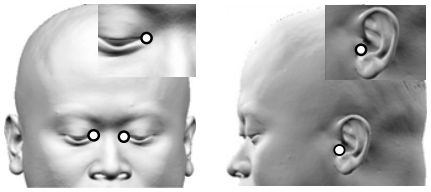

(a) (b)

Fig. 1 (a) Medial canthus and (b) tragus

II. Previous Work

The majority of work on localizing anatomical landmarks in head CT images is concerned with localizing internal landmarks of the head. Frantz et al. [2] used 3D generalizations of 2D differential operators/corner detectors to localize tips of the frontal, temporal, and occipital horns of the ventricular system; saddle point of the zygomatic bone; fourth ventricle, and tip of the external occipital protuberance. Their method is prone to false detections and requires the user to specify a coarse position of the landmark of interest as well as to select the most promising candidate among the detected candidate landmarks.

A more recent approach fits geometric and intensity models of these landmarks to their images [3], [4]. In this semi-automatic approach, the user is required to provide a coarse localization of the landmarks, which the algorithm then refines, by fitting models of anatomical structures to their images. These techniques could be applied to localizing the tragus, and to a lesser extent the medial canthus. However, user intervention, to provide coarse localization of these

M. Ovinis is a lecturer in the Department of Mechanical Engineering, Universiti Teknologi PETRONAS, 31750, Tronoh, Malaysia (phone: +6053687150; fax: +6053656461; e-mail: mark_ovinis@petronas.com.my).

D. Kerr and K. Bouazza-Marouf are Senior Lecturers in the Department of Mechanical and Manufacturing Engineering, Loughborough University, LE11 3TU, Loughborough, UK (e-mail: d.kerr@lboro.ac.uk, k.bouazza- marouf@ lboro.ac.uk, respectively).

Prof. M. Vloeberghs is a Consultant Neurosurgeon at the Queen's Medical Centre, Nottingham University, NG7 2UH, Nottingham, UK (e-mail: Michael.Vloeberghs@Nottingham.ac.uk).

landmarks, is required as well.

Recently, Subburaj et al. [5] described a method to localize anatomical landmarks of the knee-joint in CT images automatically, using surface curvature properties and the spatial adjacency of landmarks i.e. the relative location of a landmark with respect to another landmark. Their work is not applicable in our case because there are no other landmarks close to the medial canthus or tragus that can be used to facilitate their localization.

Closely related to our work is the localization of anatomical landmarks of the face in 3D range images. Deo and Sen [6] localized anatomical landmarks of the face such as the medial canthus on a surface mesh extracted from range images, using curvature analysis and morphological operations. The extremities of regions isolated by thresholding the mesh, based on a predetermined mean curvature threshold range, correspond to the landmarks. A morphological opening operator was used on these regions to isolate and group individual vertices into regions of interest. However, their method is susceptible to localization errors when more than one 'characteristic' region of the face is present. Fig. 2 shows illustrative examples of erroneously localized medial canthus positions on surface models reconstructed from CT images from our database (see Section IV), based on Deo and Sen's method [6].

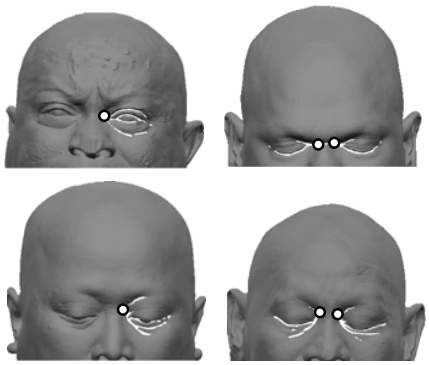

Fig. 2 Erroneously localized medial canthus based on Deo and Sen's method [6]

Although they achieved good results with their database of about 20 subjects, this was achieved with comparatively lower resolution images. In contrast, our dataset consisted of high resolution images of 102 subjects. These higher resolution images, while affording greater localization accuracy, are more susceptible to false detection. Because their intended application is in anthropometry i.e. the science and practice of human body measurements, they were primarily interested in measuring distances between landmarks, rather than localizing the landmarks accurately.

Chen et al. [7] presented a scale space non-model based approach using integral volume descriptors, for localizing anatomical landmarks of the face. Integral descriptors are more robust to noise then curvature based strategies. However, similar to the work by Deo and Sen [6], they used 3D range images. Because of its relatively low resolution, the majority of the work in the localization of anatomical landmarks of the face in 3D range images detects a region of interest, rather than a specific point. As such, although seemingly similar in nature, the context of the localization is different. In this work, the medial canthus and tragus are localized in high resolution CT images based on curvature analysis and a rule-based system. To our knowledge, no prior work to localize these landmarks in CT images has been reported.

III. Methodology

The medial canthus and tragus were localized on surface models extracted from CT images. Candidate landmark locations are isolated on the surface models based on their curvature properties. However, the use of curvature properties alone will result in numerous false detections. We use a rule-based system to facilitate the localization of the landmarks. Landmarks are localized within candidate locations that have a geometric structure and spatial location consistent with the prior knowledge of the landmarks. The various stages of the algorithm are detailed below.

A. Head Orientation

A necessary step in the algorithm is to detect and correct for any deviation of the head orientation (Fig. 3 (a)) from a forward facing position (Fig. 3 (c)). This is because the localization is based on the anatomical positions of these landmarks when the head is in an approximately forward facing position. To estimate the orientation of the head in CT images, the head region must first be segmented in the CT axial images (Fig. 3 (a)). Intensity-based thresholding works well in isolating the head region, with the threshold level determined automatically by Otsu's method. To eliminate spurious regions in the segmented images (Fig. 3 (b)), the largest connected binary component (Fig. 3 (c)), which corresponds to the head, is selected. The resulting binary CT axial images are stacked to create a composite image (Fig. 3 (d)).

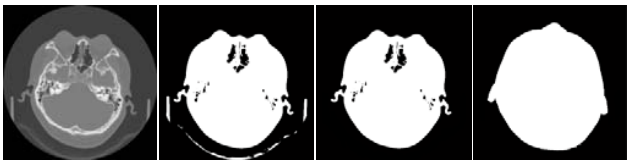

(a) (b) (c) (d)

Fig. 3 (a) Original CT axial image, (b) segmented image, (c) largest connected binary component and (d) composite image

The orientation of the head, ϕ, is then estimated as the 2D orientation of an ellipse with the same normalized second central moments as the composite image, which is approximately elliptical, using (1):

$$\emptyset = \tan^{-1}\left(\frac{\mu_{02} - \mu_{20} + \sqrt{(\mu_{02} - \mu_{20})^2 + 4{\mu_{11}}^2}}{2\mu_{11}}\right) \quad (1)$$

where $\mu_{20} = \frac{\sum(x-\bar{x})^2}{N}$, $\mu_{02} = \frac{\sum(y-\bar{y})^2}{N}$, and $\mu_{11} = \frac{\sum(x-\bar{x})(y-\bar{y})}{N}$, are the second order central moments, x and y the x and y pixel coordinates, $\bar{x}$ and $\bar{y}$ the mean x and y pixel coordinates and N the number of pixels.

The orientation estimated using this method becomes less accurate the closer the shape of the composite image is to a circular shape. This is because the terms $(\mu_{02} - \mu_{20})$ and μ_{11} become smaller, leading to numerical instability. As the head is only required to be approximately forward facing, only deviations of more than 15° from the vertical axis are corrected. If required, a rigid body rotation of the CT images, about its centroid, is used to re-orient the CT images (Fig. 4). Once properly oriented, the surface model of the head is extracted from the CT images.

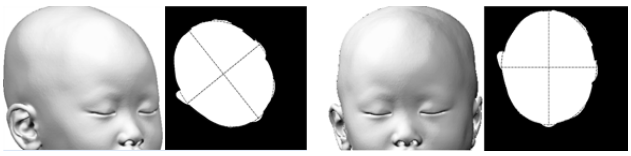

(a) (b)

Fig. 4 Surface model and corresponding stacked axial CT images (with the major and minor axis of the ellipse overlaid) illustrating deviation from (a) frontal facing position and (b) reoriented head

B. Surface Model

To obtain a surface model of the head from CT images, the binary CT axial images of the segmented head region (Fig. 3 (c)) are first multiplied with the original CT axial images (Fig. 3 (a)). A grey level morphological fill operation is then performed on the segmented image (Fig. 5 (a)) to remove any holes (Fig. 5 (b)), as they would complicate the automatic localization of the landmarks.

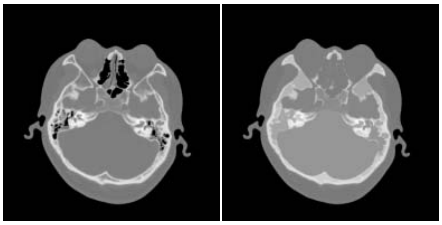

(a) (b)

Fig. 5 (a) Head region with 'holes' and (b) without 'holes' after grey level morphological fill operation

A surface model of the head, represented as a triangulated mesh, is then extracted using a custom isosurface algorithm [8], with an isovalue equal to the threshold level used for segmentation. A sample of the surface model of a head for one subject in our database, extracted from CT images, is shown as in Fig. 6. The curvature of the surface models is computed next.

Fig. 6 Sample of head surface model extracted from CT images (Frontal view and corresponding profile view)

C. Surface Curvature

Computation of the curvature of the surface model is not trivial because unlike a parametric surface, a triangulated mesh is piecewise linear and cannot be differentiated. There are three approaches to calculate the curvature of a surface represented by a mesh: fitting methods, discrete methods, and curvature tensor estimation methods. In fitting methods, which are computationally expensive, an analytic function, whose curvature can be computed, is fitted to a mesh locally. Discrete methods involve a direct estimation of the curvature at each vertex, by summing the curvature of each face or edge associated with the vertex. These methods are appealing because of their speed. However, they are sensitive to noise and mesh resolution. Curvature tensor estimation methods are similar to discrete methods, except that instead of estimating the curvature directly, a curvature tensor is estimated. Curvatures and principal directions are derived from the eigenvalues and eigenvectors of the curvature tensor. Curvature tensor estimation methods are computationally less complex than fitting methods.

A curvature estimation method by Alliez et al [9] was used to estimate the curvature of an isosurface. In their method, a curvature tensor is defined at each point along the edge, by observing that for every edge e of the mesh, the minimum curvature is along the edge, and the maximum curvature is across the edge. A curvature tensor can therefore be defined at each point along an edge. The curvature tensor, $\mathfrak{I}$ of an arbitrary region, B is the average of these individual tensors over the region. Formally, the curvature tensor, $\mathfrak{I}(v)$ at an arbitrary vertex, v on the mesh, over B is given by:

$$\mathfrak{I}(v) = \frac{1}{|B|} \sum_{edges\ e} \beta(e)|e \cap B|\bar{e}\bar{e}^t \qquad (2)$$

where $|B|$ is the surface area around v over which the tensor is estimated, $\beta(e)$ is the signed angle between the normals to the two oriented triangles incident to edge e (positive if convex, negative if concave), $|e \cap B|$ is the length of $e \cap B$ (always between 0 and $|e|$), and $\bar{e}$ is a unit vector in the same direction as e. To obtain a continuous tensor field over the whole surface, the piecewise curvature tensor is linearly interpolated at each vertex. The normal at each vertex is the eigenvector of the curvature tensor $\mathfrak{I}$ associated with the minimum eigenvalues. The principal curvatures at v, κ_{min} and κ_{max}, are the two other eigenvalues of curvature tensor $\mathfrak{I}$. The Gaussian and mean curvature can be computed from the principal

curvatures. The Gaussian curvature $C_{gaussian}$ is the product of the principal curvatures, κ_{min} and κ_{max} and is given by:

$$C_{gaussian} = \kappa_{min}\kappa_{max} \quad (3)$$

The mean curvature C_{mean} is the average of the principal curvatures, κ_{min} and κ_{max} and is given by:

$$C_{mean} = \frac{1}{2}(\kappa_{min} + \kappa_{max}) \quad (4)$$

Fig. 7 illustrates the mean curvature map of the eye and the Gaussian curvature map of the ear, determined using the curvature tensor estimation algorithm. The curvature values have been normalized and color coded for display purposes.

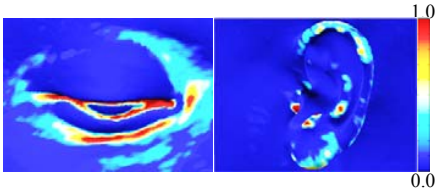

(a) (b)

Fig. 7 (a) Mean curvature map of the eye region and (b) Gaussian curvature map of the ear region

To reduce the effect of noise when estimating surface curvature, a 10-ring neighborhood averaging of the curvature tensor at each vertex was applied. Fig. 8 illustrates the effect of the neighborhood averaging size on curvature values. Curvature values are smoother as the curvature tensor is averaged over larger neighborhoods although this has the effect of masking surface detail and blurring curvature estimates.

(a) (b)

Fig. 8 Thresholded mean curvature map at (a) 0-ring and (b) 10-ring neighborhood averaging filter sizes

D.Candidate Landmark Regions

The amount and the type of curvature of a point on a surface are indicative of its local shape. However, curvature properties alone are inadequate to localize the landmarks, as there will be many false positives (Fig. 7). Instead, candidate regions that may contain the landmarks are first identified, with the landmarks subsequently localized within these regions. This is because localizing the region containing the landmarks is less error prone than localizing the landmarks by themselves.

Geometrically, the medial canthus is the most medial point of a valley surface formed by intersection of the upper and lower eyelids. This valley surface extends from the outer corner to the inner corner of the eye and is characterized by high mean curvature and zero Gaussian curvature. Candidate locations for the medial cantus are therefore isolated by thresholding the surface curvature based on mean curvature threshold, C_{mean}, and Gaussian curvature threshold, $C_{gaussian} = 0$ (Fig. 9).

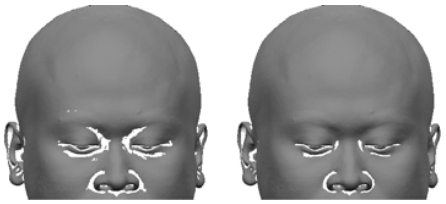

(a) (b)

Fig. 9 Curvature map with $\boldsymbol{C_{gaussian} = 0}$ and $\boldsymbol{C_{mean} \geq}$ (a) 0.005 and (b) 0.015

The tragus is approximately semi-ellipsoid, and its apex is the tip of this peak structure, a locally maximum point (Fig. 1 (b)). It is characterized by negative mean curvature and high Gaussian curvature (Fig. 7 (b)). Candidate locations containing the tragus are identified by thresholding the surface curvature based on Gaussian curvature, $C_{gaussian}$ and $C_{mean} < 0$ (Fig. 10).

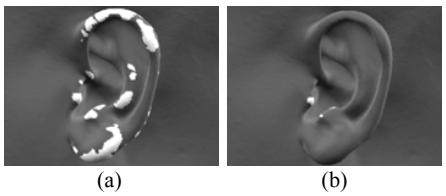

(a) (b)

Fig. 10 Curvature map with $\boldsymbol{C_{mean} < 0}$ and (a) $\boldsymbol{C_{gaussian} \geq 0.0001}$ (b) $\boldsymbol{C_{gaussian} \geq 0.0005}$

The curvature properties used are different from those used by Deo and Sen in that we use the two principal curvatures, the mean and Gaussian curvature, instead of using mean curvature only. Mean curvature alone is not very indicative of local shape. Using two principal curvatures i.e. mean and Gaussian curvature would yield more information about local shape. The curvature properties used are based on the surface geometry of the landmarks and the threshold level used is determined empirically based on our dataset. For the medial canthus, a mean curvature threshold level of $C_{mean} = 0.015$ (Fig. 9 (b)) works well in the majority of cases, although in some instances the mean curvature threshold is varied to two predefined levels i.e. $C_{mean} = 0.010$ and $C_{mean} = 0.020$. For the tragus, a Gaussian curvature threshold level of $C_{gaussian} = 0.0005$ (Fig. 10 (b)) works well. Once isolated, candidate landmark regions are clustered to facilitate landmark localization.

E. Clustering

The eyes (including the nose) and ears (Fig. 11 (a)) are first isolated using nearest neighbor clustering, with the eyes and nose area further divided into the right eye, the left eye and the nose (Fig. 11 (b)). The seed points used for the nearest neighbor clustering are based on the relative positions of these anatomies.

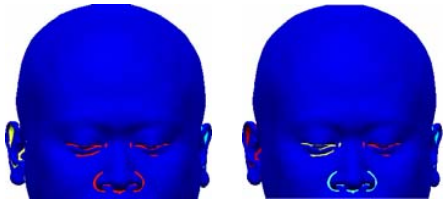

(a) (b)

Fig. 11 Nearest neighbor clustering, of (a) right ear, eyes and nose, left ear and of (b) right ear, right eye, nose, left eye and left ear

As each anatomical area will usually have more than one candidate landmark region, they will be grouped into individual clusters (Fig. 12). As the regions tend to have arbitrary shapes, density-based clustering [10], which works well with these types of shapes, is used.

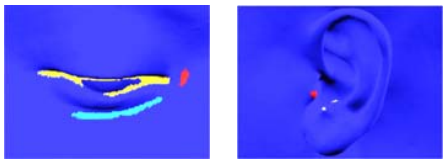

(a) (b)

Fig. 12 Density-based clustering of a thresholded surface curvature map of the (a) eye and (b) ear
Each color represents a separate cluster

F. Curve Skeleton Extraction

When multiple clusters are present in the eye region, the cluster containing the landmark has to be identified. For the medial canthus, part of the difficulty in localizing this cluster is that the shape of the cluster is different depending on whether the eyes are closed (Fig. 13 (a)), opened (Fig. 13 (b)) or partially opened (Fig. 13 (c)).

(a) (b) (c)

Fig. 13 Clusters containing the medial canthus with the eyes (a) closed, (b) opened and (c) partially opened

To identify the cluster containing the medial canthus, the curve skeleton of the clusters is extracted, and the number of branch points/nodes computed. The number of branch points of a curve skeleton is an indication of whether a cluster contains the medial canthus. Curve skeleton extraction is based either on volumetric or geometric techniques. Volumetric methods require voxelization/discretization of the cluster, resulting in lower resolution and loss of detail. On the other hand, geometric methods work directly on triangle meshes. Fig. 14 illustrates the curve skeleton of the clusters in the eye region, based on a geometric method by Cao et al [11].

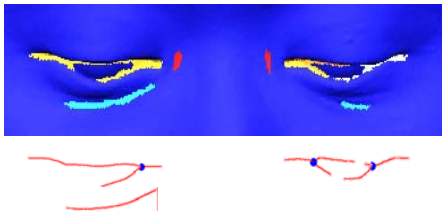

Fig. 14 Clusters of a thresholded surface curvature map of the eye region and the corresponding curve skeleton. Branch points are indicated as nodes

The curve skeletons are extracted from each cluster individually to avoid points belonging to different clusters combining into a single curve skeleton. The goal is to determine if any of the clusters has curve skeletons with two branch points, as this corresponds to the geometry of a cluster with the eyes open or partially opened, and is therefore the cluster containing the medial canthus. Fig. 15 illustrates the corresponding branch points of the curve skeleton of the clusters around the eye, at $C_{mean} = 0.015$ and $C_{mean} = 0.010$ ($C_{gaussian} = 0$). Based on the initial mean curvature threshold, $C_{mean} = 0.015$, neither cluster contains two branch points (one cluster contains a branch point and the other cluster contains no branch point), as illustrated in Fig. 15 (a). Decreasing the threshold, $C_{mean} = 0.010$, yields a cluster containing two branch points (Fig. 15 (b)). The medial canthus corresponds to the most medial point of the cluster corresponding to the curve skeleton with two branch points. If no cluster with a curve skeleton containing two branch junctions is found, the process is repeated with $C_{mean} = 0.020$.

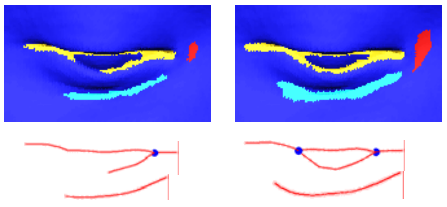

(a) (b)

Fig. 15 Clusters and the corresponding curve skeletons for $\boldsymbol{C_{gaussian} = 0}$ and mean curvature threshold (a) $\boldsymbol{C_{mean} \geq 0.015}$ and (b) $\boldsymbol{C_{mean} \geq 0.010}$

If a cluster with a curve skeleton containing two branch junctions is still not found, the eyes are either closed or partially opened. In this case, the cluster whose curve skeleton

is the longest, based on the initial threshold, is the cluster containing the medial canthus (Fig. 16 (a)).

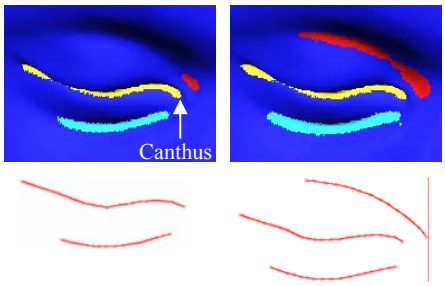

(a) (b)

Fig. 16 Clusters and corresponding curve skeletons for $\boldsymbol{C_{gaussian}} = \mathbf{0}$ and mean curvature threshold (a) $C_{mean} \geq 0.015$ and (b) $C_{mean} \geq 0.010$

Curve skeleton length is a more appropriate measure than the Euclidean distance between the two extreme points of a cluster because it takes into account the surface shape. A curve skeleton with single branch point (Fig. 17 (a)) does not correspond to the cluster containing the medial canthus. This simplistic approach to localizing the cluster containing the medial canthus works well with the images in our dataset. For the extraction of curve skeletons, three mean curvature threshold values, $C_{mean} = 0.010, 0.015$ and 0.020 were used. The default threshold used is 0.015, with the threshold decreased to $C_{mean} = 0.010$ or increased to $C_{mean} = 0.020$ (Fig. 17 (b)) depending on whether a cluster containing the medial canthus is found. A threshold based on an arbitrary upper limit of a curvature histogram was considered but the presence of outliers due to an imperfect segmentation e.g. parts of the headrest, greatly affected the resulting threshold value.

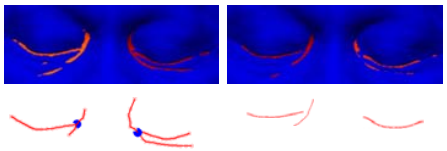

(a) (b)

Fig. 17 Curve skeletons for $C_{gaussian} = 0$ and mean curvature (a) $C_{mean} \geq 0.015$ and (b) $C_{mean} \geq 0.020$. Only main curve skeletons are shown

G.Algorithm for the Localization of the Medial Canthus

Input: CT images

1) Reorient the head if the head orientation in the axial plane deviates more than 15° from the forward facing position (see Fig. 4).
2) Extract surface model of head from CT images (see Fig. 6).
3) Compute surface curvature (see Fig. 7)
4) Find candidate vertices, $v_j \in V\{j = 1,2,\dots,n\}$ by thresholding based on $C_{mean} \geq 0.015$ and $C_{gaussian} = 0$ (see Fig. 9 (b)).
5) Group each vertex; $v_j \in C_i\{i = 1,2,3\}$ into clusters using density based clustering (Fig. 12).
6) Isolate resulting clusters, corresponding to the left ear, the eye and nose, and the right ear, using nearest neighbor clustering (see Fig. 11 (a)).
7) Separate the eye and nose, $d_j \in c_2\{i = 1,2,3\}$ into three clusters, corresponding to the left eye, the nose and the right eye, using nearest neighbour clustering (see Fig. 11 (b)).
8) If there is no candidate cluster for the eye i.e. d_1 and/or d_3, go back to step 1 but change the mean curvature threshold to 0.010.
9) If there is only one candidate cluster for the eye, select the cluster, $e_1 \in d_1$ and $e_2 \in d_3$ if it has either no branch points or two branch points. Otherwise, go back to step 2 but change mean curvature threshold to 0.020 in the first instance and 0.010 in the second instance. If there is more than one candidate cluster (see Figs. 14–17), select the cluster, $e_1 \in d_1$ and $e_2 \in d_3$ that has two branch points (see Fig. 15 (b)). Otherwise, go back to step 2 but threshold using $C_{mean} \geq 0.010$ in the first instance and $C_{mean} \geq 0.020$ in the second instance.
10) If no cluster containing two branch points is found, the cluster with the longest curve skeleton length, based on $C_{mean} \geq 0.015$, is selected as the cluster containing the medial canthus (see Fig. 16 (a)).
11) Select most medial vertex, $v_{lmc} \in e_1$for left medial canthus and most medial vertex, $v_{rmc} \in e_2$ for right medial canthus.

Output: Vertices corresponding to the left and right medial canthus $\{v_{lmc}, v_{rmc}\}$.

H.Estimating the Tragus Location

To facilitate the localization of the tragus and to avoid large localization errors, the location of the tragus is first estimated (Fig. 18). This is because the ear region sometimes contains multiple clusters due to the presence of other structures, such as the headrest and straps of the breathing mask, as a result of imperfect segmentation (Fig. 19).

Fig. 18 Estimated tragus positions

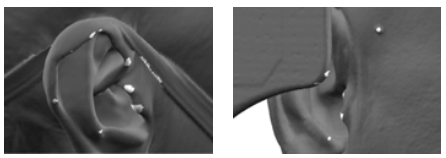

(a) (b)

Fig. 19 Thresholded Gaussian curvature map of the ear with negative mean curvature illustrating (a) noise and (b) part of the ear truncated in the surface model

The position of the tragus is estimated by looking for the presence of ear canals in the CT axial (Fig. 20 (b)) and coronal planes (Fig. 20 (c)); and the outer ear structure in the CT sagittal plane (Fig. 21).

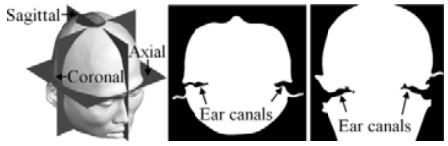

(a) (b) (c)

Fig. 20 (a) Anatomical planes of reference, (b) ear canals in CT axial plane and (c) ear canals in CT coronal plane

The sagittal plane where the tragus is approximately located may be found by scanning from the most lateral to the most medial sagittal plane (Fig. 21) until the Euler number of the largest connected binary region is equal to or is less than zero. In practice, morphological operations need to be performed to avoid false detections.

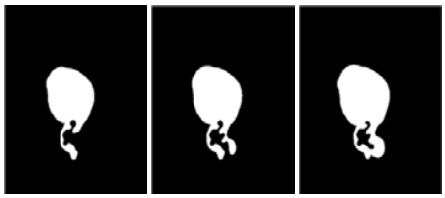

Fig. 21 (from left to right) Sequence of the outer ear structure in CT sagittal view i.e. lateral to medial

The ear canals in the axial and coronal CT planes are prominent features that can be robustly localized by skeletonization (Fig. 22). The axial and coronal planes whose skeleton endpoints are closest to the mid-sagittal plane correspond to the axial and coronal planes where the tragus is approximately located.

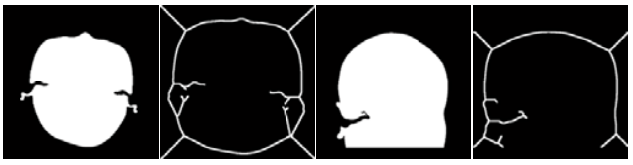

(a) (b) (c) (d)

Fig. 22 (a) Ear canals in CT axial plane, (b) corresponding image skeleton, (c) ear canals in CT coronal plane and (d) corresponding image skeleton

The largest cluster, within 10 mm from the estimated tragus location, is selected as the cluster containing the tragus. The 10 mm figure was determined empirically based on our database. The vertex with the highest Gaussian curvature value in this cluster corresponds to the apex of the tragus.

I. Algorithm for the Localization of the Tragus

Input: CT images

1) Reorient the head if the head orientation in the axial plane deviates more than 15^o from the forward facing position (see Fig. 4).
2) Extract surface model of head from CT images (see Fig. 6).
3) Compute surface curvature (see Fig. 7)
4) Estimate location of the tragus (see Fig. 18). This corresponds to the axial (see Fig. 20 (b)) and coronal (see Fig. 20 (c)) plane where the ear canals appears longest based on skeletonisation (see Fig. 22), and the first sagittal plane (from lateral to medial), with a region whose Euler number is equal to, or less than, zero (see Fig. 21.
5) Find candidate vertices, $v_j \in V_i \{j = 1,2,\dots,n\}$ by thresholding based on $C_{gaussian} \geq 0.0005$, and $C_{mean} < 0$ (see Fig. 10 (b)).
6) Group each vertex, v_j, into clusters, $C_k \{k = 1,2,\dots.,p\}$ using density based clustering (see Fig. 12 (b))
7) Select the largest cluster, $c \in C_k \{k = 1,2,\dots.,p\}$, within 10 mm from the estimated tragus location.
8) The vertices, $v_{lt}, v_{rt} \in c$ with the highest Gaussian curvature value correspond to the apex of the left and right tragus respectively.

Output: Vertices, $\{v_{rt}, v_{lt}\}$, corresponding to the left and right tragus.

J. Overview of the Automatic Localization Algorithm

The various stages in the algorithm are shown in flowchart form in Fig. 23.

IV. Results

A dataset consisting of near isotropic CT images of 118 patients acquired using a Toshiba Aquilion 16 CT scanner was used to test the algorithm. CT images of 16 patients (out of 118 patients) were discarded from the analysis because the medial canthus or tragus was either not present or well-defined in the CT images. Of the 102 patients that were included in the analysis, 52 patients were scanned with their eyes opened or partially opened, with the remaining 50 patients scanned with their eyes closed. There was no significant difference between the localization errors for the two groups of patients. The images are 512 x 512 pixels with average in-slice pixel spacing and average slice thickness of 0.5 mm each, with no interslice spacing. The start and end scan location is from the skull vertex to at least the skull base, with the gantry oriented parallel to the infraorbitomeatal line (without any tilt). The DICOM compliant CT images were transferred to a personal computer, and the landmarks were localized automatically. Fig. 24 illustrates the automatically localized medial canthus and the apex of the tragus for eight subjects in our database.

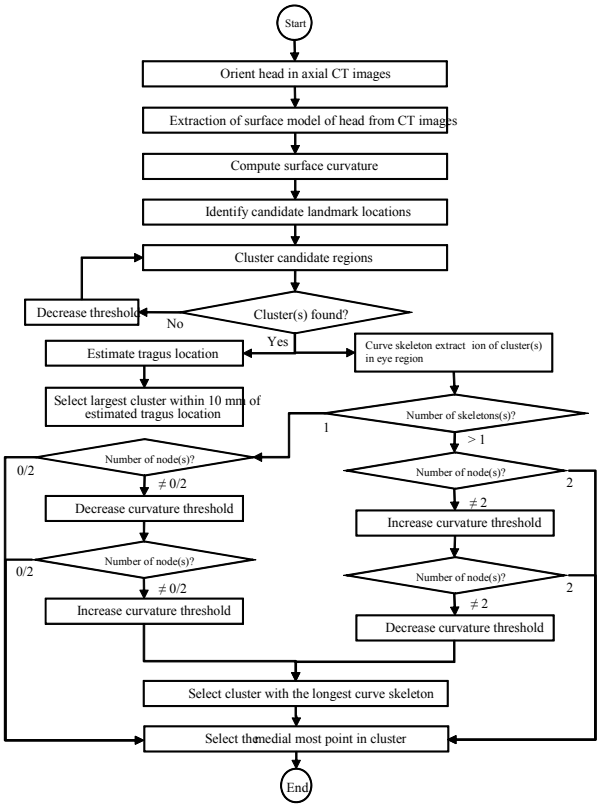

Fig. 23 Overview of the algorithm

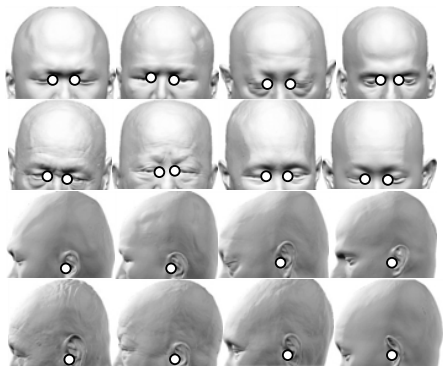

Fig. 24 Automatically localized medial canthus and the apex of the tragus

Because of the retrospective nature of this validation, there is no anatomical ground truth. As such, the difference in localizing the landmarks, defined as the distance between the perceived location of the landmark (as determined by visual inspection on the surface rendered model) and the location of the landmark found automatically based on the algorithm was used for comparison. Because manual localization is subjective and is a function of the examiner's experience and perception, to minimize bias the landmarks were annotated twice and their position were averaged. Intra examiner variability was 1.0 mm and 0.7 mm for the medial canthus and tragus, with a maximum variability of 2.9 mm and 2.5 mm respectively.

The mean difference in the localization of the medial cantus, expressed as the root mean square Euclidean distance, was 1.5mm, with a maximum difference of 4.5mm. The mean difference for localizing the tragus was 0.8mm with a maximum difference of 2.6mm. For the medial canthus, automatic and manual localization agreed to within 1mm for 51% of the landmarks, within 2mm for 80% of the landmarks, within 3mm for 89% of the landmarks, and within 4mm for 94% of the landmarks. For the tragus, automatic and manual localization agreed within 1mm for 75% of the landmarks, and within 2mm for 97% of the landmarks. Estimates of the tragus location were found to be always within 10mm of its actual location, with an average difference of 8-mm.

V. Discussions and Conclusion

Recent advances in scanner technology have made high resolution CT images routinely available. These images can be reconstructed retrospectively from existing raw data, without re-scanning the patient, with the only limitation being the detector configuration used during the scan. Isotropic or near isotropic sub-millimeter resolution mean that CT images could now achieve a level of detail that has made possible the detection of point landmarks that would be unfeasible in low-resolution images. We compared the results for the localization of the medial canthus with that reported by Deo and Sen. To compare our results with theirs, we computed the distance between the two medial canthus i.e. intercanthal width, for the automatically and manually localized medial canthus. Their manual measurements are ground truth measurements, based on measuring the medial canthus on the subject using calipers. Deo and Sen obtained an error of 0.85% for the difference between the intercanthal widths determined automatically and manually for one subject, compared to an average error of 3.8% for 102 subjects based on our technique.

Good measurement accuracy however, does not necessarily correspond to accurate landmark localization. This is because landmarks can be erroneously localized but the distance between the landmarks could still be accurate e.g., the localization of both landmarks could be offset by equal amounts. Furthermore, because we are primarily interested in using these landmarks as a basis to register images from two different modalities, the localized landmarks have to be spatially consistent between the two modalities. As such, localization accuracy rather than measurement accuracy is a more meaningful measure.

The maximum difference in positions of landmarks localized manually and automatically of 4.5mm for the medial canthus and 2.6 mm for the tragus is acceptable. This is because the error in localizing a target, or the target registration error (TRE), for this landmark localization error is within the clinical accuracy required for the three targeted neurosurgical procedures [12] (as determined using an analytical expression by Fitzpatrick et al [13]).

A methodology to localize the medial canthus and tragus in

CT images automatically was presented. The basic approach was to exploit the curvature saliency of the medial canthus and tragus, as they are the most geometrically salient among commonly used anatomical landmarks of the head, and can therefore be more reliably detected. A rule system based on prior knowledge of the landmark geometric structure and spatial location was used to constrain the landmark search, as curvature properties alone results in many false detections.

Because the localization is complex, a heuristic approach was adopted. Heuristics are often used in localizing facial landmarks, often producing better results than statistical methods [14]. Although the technique developed may not extend easily to other anatomical landmarks, general landmark localization algorithms [2]-[4] requires user intervention. In this work, the intended application is for an automated image to patient registration system, whereby the end user is only required to validate the localization., the user can this prior to the registration and surgical intervention.

Future work includes developing a framework in a clinical setting for an end-user to verify and in the event of large localization errors, correct the automatically localized landmarks. The localization of other anatomical landmarks will also be investigated, as registration accuracy in general improves when more landmarks are used (if there is no systematic bias error in identifying the landmarks). Finally, the localization of the medial canthus and tragus in other imaging modalities, such as magnetic resonance imaging, will be explored.

REFERENCES

[1] M. Gooroochurn, D. Kerr, K. Bouazza-Marouf and M. Ovinis. Facial Recognition Techniques Applied to the Automated Registration of Patients in the Emergency Treatment of Head Injuries. P. I. Mech. Eng. H. Med., 225, 2011, pp. 170-180.

[2] S. Frantz, K. Rohr and H. S. Stiehl. Development and Validation of A Multi-Step Approach to Improved Detection of 3D Point Landmarks in Tomographic Images. Image Vision Comput., 23, 2005, pp. 956-971.

[3] Frantz S, Rohr K and Stiehl HS. Localization of 3D Anatomical Point Landmarks in 3D Tomographic Images Using Deformable Models. Lect Notes Comput Sc., 2000. pp. 492-501.

[4] S. Wörz and K. Rohr. Localization of Anatomical Point Landmarks in 3D Medical Images by Fitting 3D Parametric Intensity Models. Med. Image Anal., 10, 2006, pp. 41-58.

[5] K. Subburaj, B. Ravi and M. Agarwal. Automated Identification of Anatomical Landmarks on 3D Bone Models Reconstructed From CT Scan Images. Comput. Med. Imaging Graphics., 33, 2009, pp. 359-368.

[6] D. Deo and D. Sen. Mesh Processing for Computerized Facial Anthropometry. J. Comput. Inf. Sci. Eng., 10, 2010, pp. 1-12.

[7] D. Chen, G. Mamic , C. Fookes , S. Sridharan. Scale-Space Volume Descriptors for Automatic 3D Facial Feature Extraction. Int. J. Signal Processing., 5, 2009, pp. 264-269.

[8] The MathWorks, Source Code for the Matlab Isosurface Function. 2007.

[9] P. Alliez, D. Cohen-Steiner, O. Devillers, B. Lévy and M. Desbrun. Anisotropic Polygonal Remeshing," ACM T. Graphic. 22, pp. 485-493.

[10] M. Ester, H. P. Kriegel, J. Sander and X. Xu. A Density-Based Algorithm for Discovering Clusters in Large Spatial Databases with Noise. Proc., 2nd Int. Conf. on Knowledge Discovery and Data Mining, 1996, pp. 226-231.

[11] J. Cao, A. Tagliasacchi, M. Olson, H. Zhang and Z. Su. Point Cloud Skeletons via Laplacian Based Contraction. Shape Modeling Int. Conf., 2010, pp. 187-197.

[12] M. Gooroochurn, M. Ovinis, D. Kerr, K. Bouazza-Marouf and M. Vloeberghs. A Registration Framework for Preoperative CT to Intraoperative White Light Images. Medical Image Understanding and Analysis, 2009, pp. 184-188.

[13] J. M. Fitzpatrick and J. B. West. The Distribution of Target Registration Error in Rigid-Body Point-Based Registration. IEEE Trans. Med. Imag., 20, pp.917-927.

[14] A. A. Salah and L. Akarun. 3D Facial Feature Localization for Registration. Lect Notes Comput Sc., 4105, 2006, pp. 338-345.